Cell Cycle

ISSN: 1538-4101 (Print) 1551-4005 (Online) Journal homepage: https://www.tandfonline.com/loi/kccy20

Cell cycle and differentiation of Sca-1^{+} and Sca-1^{-} hematopoietic stem and progenitor cells

Petr Páral, Kateřina Faltusová, Martin Molík, Nicol Renešová, Luděk Šefc & Emanuel Nečas

To cite this article: Petr Páral, Kateřina Faltusová, Martin Molík, Nicol Renešová, Luděk Šefc & Emanuel Nečas (2018) Cell cycle and differentiation of Sca-1^{+} and Sca-1^{-} hematopoietic stem and progenitor cells, Cell Cycle, 17:16, 1979-1991, DOI: 10.1080/15384101.2018.1502573

To link to this article: https://doi.org/10.1080/15384101.2018.1502573

CELL CYCLE
2018, VOL. 17, NO. 16, 1979–1991
https://doi.org/10.1080/15384101.2018.1502573

Taylor & Francis
Taylor & Francis Group

RESEARCH PAPER

Cell cycle and differentiation of Sca-1$^+$ and Sca-1$^-$ hematopoietic stem and progenitor cells

Petr Páral [a], Kateřina Faltusová [a], Martin Molík [a], Nicol Renešová [a,b], Luděk Šefc [c], and Emanuel Nečas [a,b]

[a]First Faculty of Medicine, Institute of Pathological Physiology, Charles University, Prague, Czech Republic; [b]BIOCEV, Biotechnology and Biomedicine Center of the Academy of Sciences and Charles University in Vestec, Institute of Pathological Physiology, Charles University, Czech Republic; [c]Center for Advanced Preclinical Imaging, First Faculty of Medicine, Charles University, Prague, Czech Republic

ABSTRACT

Hematopoietic stem and progenitor cells (HSPCs) are crucial for lifelong blood cell production. We analyzed the cell cycle and cell production rate in HSPCs in murine hematopoiesis. The labeling of DNA-synthesizing cells by two thymidine analogues, optimized for *in-vivo* use, enabled determination of the cell cycle flow rate into G2-phase, the duration of S-phase and the average cell cycle time in Sca-1$^+$ and Sca-1$^-$ HSPCs. Determination of cells with 2n DNA content labeled in preceding S-phase was then used to establish the cell flow rates in G1-phase. Our measurements revealed a significant difference in how Sca-1$^+$ and Sca-1$^-$ myeloid progenitors self-renew and differentiate. Division of the Sca-1$^+$ progenitors led to loss of the Sca-1 marker in about half of newly produced cells, corresponding to asymmetric cell division. Sca-1$^-$ cells arising from cell division entered a new round of the cell cycle, corresponding to symmetric self-renewing cell division. The novel data also enabled the estimation of the cell production rates in Sca-1$^+$ and in three subtypes of Sca-1$^-$ HSPCs and revealed Sca-1 negative cells as the major amplification stage in the blood cell development.

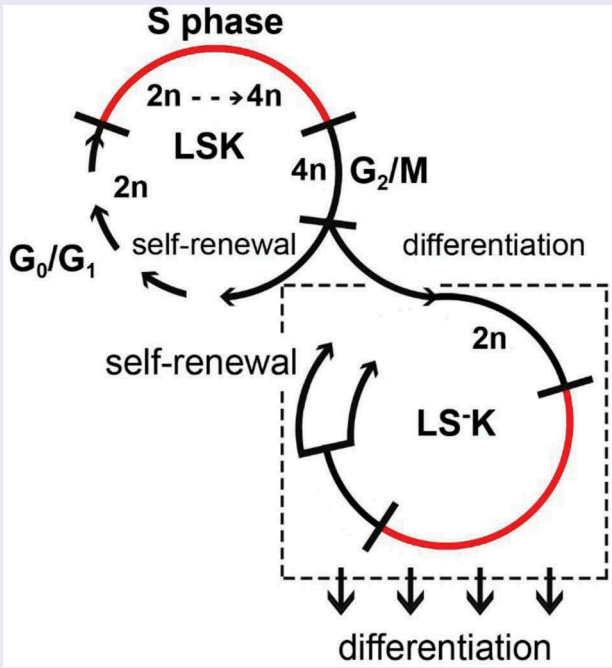

ARTICLE HISTORY
Received 6 February 2018
Revised 22 June 2018
Accepted 7 July 2018

KEYWORDS
Hematopoiesis; stem cells; progenitors; cell cycle; mouse; blood cell production

CONTACT Petr Páral petr.paral@lf1.cuni.cz
Supplementary data can be accessed here.

Introduction

Hematopoiesis is a highly efficient cell-producing system with a hierarchical structure consisting of hematopoietic stem cells (HSCs) at the apex, progenitors in the middle and differentiated precursors of blood cells at the bottom.

The introduction of flow cytometry into experimental studies of hematopoietic tissue enabled the identification of various types of immature hematopoietic cells (HSPCs) including HSCs and several types of multipotent and lineage-restricted hematopoietic progenitors and provided sophisticated research tools for their study [1–12].

The sustained production of blood cells is the principal function of hematopoietic tissue. In mice, approximately 300 million bone marrow cells generate 200–250 million of various types of myeloid blood cells every day [13,14]. Traditionally, this enormous blood cell production had been thought to depend on the activity of HSCs, which divide infrequently but maintain their population size by self-renewing cell divisions. The capacity for self-renewing cell divisions, either asymmetric or symmetric, had been regarded as a specific feature of HSCs that is lost with their differentiation.

However, this traditional view stressing a fundamental role of HSCs in the lifelong blood cell production, due to their exquisite self-renewing capacity, has been recently challenged by novel experimental data. Sun et al. [15] demonstrated that the steady-state hematopoiesis in normal adult mice is maintained by a large pool of progenitors and the contribution from HSCs, if any, is negligible. Qiu et al. [16] demonstrated that the hematopoietic stem cell that resumed active proliferation after a long period of quiescence was destined for extinction. Busch et al. [17] concluded that steady-state hematopoiesis is largely maintained by self-renewable progenitors downstream of HSCs. Hematopoiesis has also been shown to perform well in mice with a significantly reduced pool of HSCs [18]. However, Sawai et al. [19] and Akinduro et al. [20] found evidence for the participation of HSCs in the maintenance of long-term steady-state hematopoiesis, which further stressed the importance of understanding how HSPCs accomplish their role in blood cell production.

In this study, we adapted and refined the cell cycle analysis by the dual-pulse sequential labeling of DNA using two thymidine analogues, and applied it to the analysis of HSPCs in the bone marrow of mice *in situ*. Next we introduced determination of the cells arising in mitosis and maintaining their phenotype. This novel approach revealed significant differences in the cycling activities of various types of HSPCs, provided new data regarding their cell cycle characteristics, uncovered the dominant ways by which they self-renew and differentiate, and enabled estimation of their cell production rates.

Materials and methods

Experimental animals

Male and female C57BL/6J mice 6–12 weeks of age were used in this study. Mice were bred under specific pathogen-free conditions. The experiments were approved by the Laboratory Animal Care and Use Committee of the First Faculty of Medicine, Charles University; and the Ministry of Education, Youth and Sports of the Czech Republic (MSMT-6316/2014–46).

Bone marrow collection

Bone marrow was flushed from femurs with ice-cold solution of 1% bovine serum albumin (Albumin Fraction V, biotin free, Carl Roth, Germany) in phosphate-buffered saline (PBS/BSA) prepared in the laboratory. Cell concentration was measured with a Cellometer^{TM} Auto T4 automated cell counter (Nexcelom Bioscience LLC., USA).

Immunophenotype of HSPCs

Bone marrow cells (4 x 10^6) were pelleted by centrifugation (400 g, 5 min, 4°C) and cells in the pellet were stained with a combination of fluorochrome-conjugated antibodies against lineage markers (B220, CD3, Gr-1, Mac-1, Ter119), and markers for distinguishing immature hematopoietic cells (Sca-1, c-Kit, CD48, CD150, IL7R, CD16/32 (FcγRIII/II), CD34). All antibodies were purchased from BioLegend (CA, USA) and are specified in supplementary Table 1. The staining procedure was comprised of the incubation of cells with the respective antibody mixtures (20 min on ice in dark) and washing with PBS/BSA.

Percentage of DNA-synthesizing cells determined by in-vitro labeling

An APC BrdU Flow kit (BD Biosciences, USA) was used to determine the percentage of various types of HSPCs engaged in DNA synthesis, i.e. in the S-phase of the cell cycle. Four million bone marrow cells were incubated for 45 min *in-vitro* in 2 ml IMDM medium (Sigma Aldrich, USA) containing 10 μM BrdU (5-bromo-2′-deoxyuridine) (37°C, 5% CO_2 atmosphere). The whole procedure was performed according to the APC BrdU Flow kit instructions.

Cell cycle analysis after in-vivo labeling of DNA-synthesizing cells

To determine the cell flow rate into the G2-phase of the cell cycle, dual thymidine analogues sequential DNA-labeling was applied [21,22]. The combination of EdU (5-ethynyl-2′-deoxyuridine) and BrdU was used, and the method had to be optimized for use *in-vivo* (see Results part 2). EdU (1.5 mg/mouse) and BrdU (2 mg/mouse) were administered intravenously (i.v.) separated by a time interval (T_I). Bone marrow was collected into an ice-cold PBS/BSA precisely 30 minutes after BrdU administration, stained with antibodies against surface markers, and the APC BrdU Flow Kit was used to process DNA-labeled cells. BrdU was detected by anti-BrdU antibody (MoBU-1 clone, Thermo Fischer Scientific, USA) that is highly specified to BrdU, and EdU detection was performed with a Click-iT™ Plus EdU Alexa Fluor 488 Flow Cytometry Assay Kit (Thermo Fischer Scientific, USA) chemistry. The G2 cell flow rate was indicated by the percentage of EdU^+BrdU^- cells.

To determine the cell flow rate into the G1-phase of the cell cycle, mice were i.v. injected with 1 mg/mouse of BrdU, and after various time intervals (1.5–4.5 hours) bone marrow was collected into ice-cold PBS/BSA. Bone marrow cells were then stained with antibodies for the identification of various types of HSPCs, their DNA content was stained with 7AAD. The cell-bearing BrdU labels were stained with an APC BrdU Flow Kit and the percentage of diploid cells with 2n DNA content and positive for BrdU were determined by flow cytometry to distinguish between diploid G1/G0 cells and tetraploid G2 cells. The cell flow into the G1-phase was calculated from the change in the percentage of $BrdU^+$ diploid (2n) cells occurring in the period 1.5–4.5 hours after BrdU administration.

Flow cytometry

Stained bone marrow cells were analyzed using a digital FACS Canto II flow cytometer, equipped with 405 nm (60 mW), 488 nm (20 mW) and 633 nm (15 mW) lasers and the relevant configuration of optical filters and signal detectors (BD Biosciences, USA), and a FACSAria IIu cell sorter (BD Biosciences, USA) equipped with 489 nm (50 mW), 561 nm (100 mW), 638 nm (140 mW), 404 nm (100 Mw) and 355 nm (20 mW) lasers. BD FACSDiva software version 6.1.3 was used for data acquisition. CS&T beads (BD Biosciences, USA) were used for the automated cytometer setup and the performance tracking procedure before measurements. The proper compensation matrix was created by running single-stained control samples (automatic compensation). The compensation matrix was then checked and manually adjusted (if necessary) at each measurement. The generated flow cytometry data were analyzed using FlowJo vX software (FlowJo, Tree Star, USA). Debris, red blood cells and dead cells were excluded from the analysis by gating the FSC-A/SSC-A dot plot. For cell doublet discrimination, a FSC-A/FSC-H dot plot was used. To properly interpret flow cytometry data, Fluorescence-Minus-One (FMOs) controls were used for gating.

Imaging flow cytometry

Stained bone marrow cells were analyzed using 12 channels system AMNIS ImageStream X Mark II cytometer, equipped with 375 nm, 405 nm, 488 nm, 561 nm, 642 nm and 785 nm lasers under 40x software magnification. INSPIRE system software (part number: 780–01286-01, Rev. B) was used for data collection. IDEAS analysis software (v.6.1), was used for the analysis of collected data. The SpeedBead ImageStream X calibration reagent was used to calibrate the instrument before measurement by the automated suite of the systemwide ImageStreamX tests module. Fluorescence signal compensation (if necessary) was done according

to the IDEAS user manual. All instrumentation, softwares and reagents were from Amnis – EMD Millipore (USA).

Statistical analysis

Statistical analysis was performed with GraphPad Prism version 5 (GraphPad Software, CA, USA). Values are presented as mean ± standard error of the mean (SEM). Two-way analysis of variance (ANOVA) was used to compare each group to the control group (part 1 of Results). One-sample, two-tailed Student´s t-test was used to evaluate statistical significance against the theoretical expected values (part 2 of Results). P values < 0.05 were considered statistically significant. * $P < 0.05$; ** $P < 0.01$; *** $P < 0.001$.

Results

The fraction of DNA-synthesizing cells is a characteristic feature of HSPC subpopulations

We determined pulse BrdU incorporation into immature bone marrow cells lacking lineage markers (Lin^-) and highly positive for c-Kit (LK cells) in 8 independent experiments, using 8 male and 8 female C57BL/6J mice in total. These cells were divided according to the expression of the Sca-1 marker into $Sca\text{-}1^+$ (LSK) and $Sca\text{-}1^-$ (LS^-K) subpopulations. LSK cells were further divided into four subpopulations according to their CD150 and CD48 expression patterns: hematopoietic stem cells (HSCs) $CD150^+CD48^-$, multipotent progenitors (MPPs) $CD150^-CD48^-$, and heterogeneous restricted progenitors (HPCs-1 and HPCs-2) $CD150^-CD48^+$ and $CD150^+CD48^+$, respectively [8,10]. LS^-K cells lacking IL7R were characterized by CD34 and CD16/32 (FcγR III/II) markers as CMPs (common myeloid progenitors), GMPs (granulocyte-macrophage progenitors) and MEPs (megakaryocyte-erythroid progenitors) [5] (for gating see Figure 1(a)).

The BrdU positive cells indicating the S-phase fraction of DNA-synthesizing cells ranged from 2.5 ± 0.6% in MPPs to 64.8 ± 2.3% in MEPs (Figure 1(b,c)). There was no significant difference in the percentage of cells in the S-phase between male and female mice. To check the consistency of these proliferation characteristics of various types of immature hematopoietic cells, we analyzed LSK subpopulations in an additional four independent experiments comprised of untreated male and female mice of various ages (Supplementary Figure 1).

Interesting is the very low proliferation rate in relatively abundant MPPs which has been a constant finding through our experiments.

Refinement of the EdU-BrdU technique for determination of the S-phase duration and cell flow rate into G2-phase of cell cycle in HSPCs

We used the dual EdU-BrdU labeling technique to determine the duration of S-phase (T_S), cell flow rate into the G2-phase, and an average duration of the cell cycle (T_C) to further characterize the cell cycle features of HSPCs and to estimate their production rate. To avoid a prolonged incubation of bone marrow in the presence of halogenated DNA-labeling compounds and obtain thus data for cells imbedded in their natural tissue microenvironment, we decided to label HSPCs by injecting EdU and BrdU to mice *in-vivo*. The sequential labeling procedure with EdU and BrdU had to be optimized, due to the fact that the duration of the drugs' availability after their administration was unknown.

EdU and BrdU injection were separated by a time interval T_I and bone marrow cells were collected 0.5 hours after BrdU injection. The EdU^+BrdU^- cell fraction represents the cells leaving the S-phase during T_I, while the EdU^-BrdU^+ cell fraction represents the cells entering the S-phase after BrdU administration. With T_I set at 2 hours (Figure 2(a)), the ratio between EdU^+BrdU^- and EdU^-BrdU^+ (E/B ratio) cells ranged from 0.97 to 1.64 (Figure 2(d), left column). This was significantly less than its expected value of 4.0 corresponding to the fourfold longer time after EdU administration compared to that after BrdU administration. This demonstrated that EdU was not available to DNA-synthesizing cells for the entire 2-hour period preceding BrdU administration.

To achieve the labeling of all DNA-synthesizing cells with EdU, i.e. those synthesizing DNA at the time of EdU administration and those which initiated DNA synthesis during the T_I interval preceding BrdU administration, we injected mice with a second dose

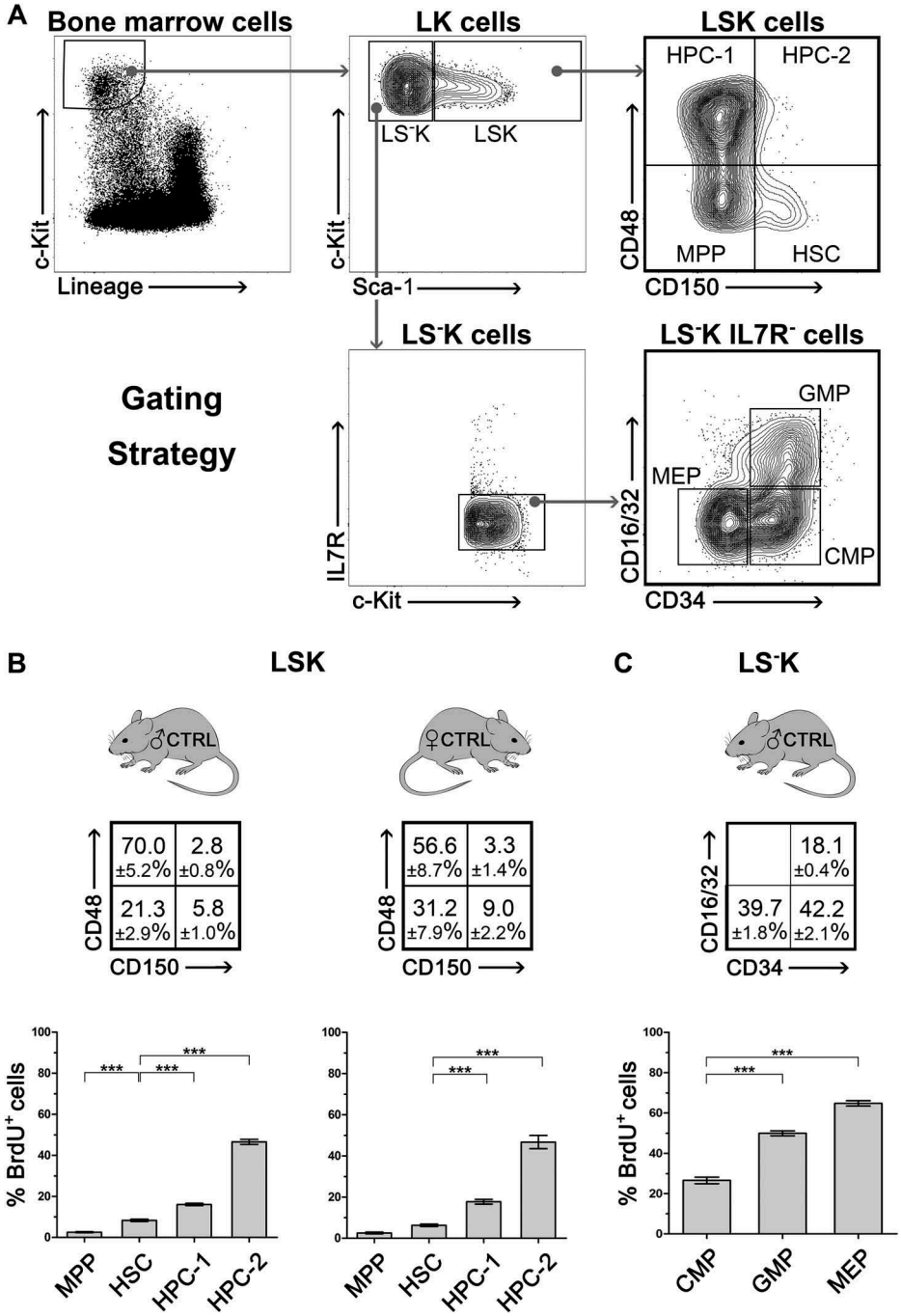

Figure 1. Frequency and proliferation rate of various subtypes of LSK and LS-K cells, and their proliferation rate A, *Gating strategy of LK cells and of their subtypes in the Sca-1$^+$ and Sca-1$^-$ fractions: HSC, MPP, HPC-1, HPC-2 and CMP, GMP, MEP*. B, *The frequency of HSC, MPP, HPC-1, HPC-2 in bone marrow of 8 male and 8 female mice and their BrdU$^+$ (S-phase) fraction after forty-five-minute in-vitro exposure to BrdU. Significant differences to HSCs (CD150$^+$CD48$^-$ cells) are marked *** ($p < 0.001$)* C, *The proportion of CMP, GMP and MEP cells in bone marrow of 4 male mice and their BrdU$^+$ (S-phase) fraction after forty-five-minute in-vitro exposure to BrdU. Significant differences to CMPs are marked *** ($p < 0.001$).*

of EdU 0.5 hours before injecting BrdU (see Figure 2 (b)). With this modification the E/B ratio slightly exceeded the theoretical value of 4.0 when T_I was still set at 2 hours. We hypothesized that this E/B ratio exceeding 4.0 was caused by overestimation of the EdU$^+$BrdU$^-$ cell fraction due to mitotic division in some of these cells during 2.5 hours after the first EdU dose. After shortening T_I to 1.5 hours, the E/B ratio achieved the expected theoretical value of 3.0 (Figure 2(d) middle and right columns). Figure 2(c)

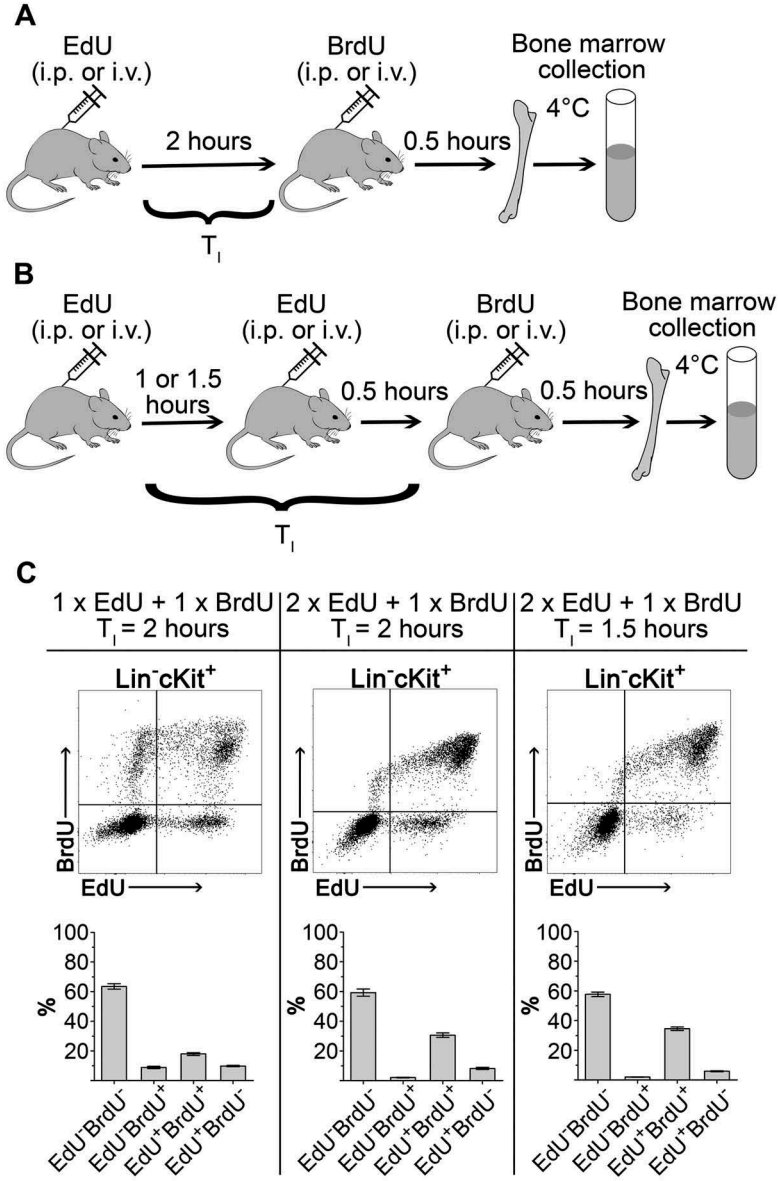

D

	(EdU⁺BrdU⁻) / (EdU⁻BrdU⁺) ratio		
	T_I = 2 hours expected value = 4		T_I = 1.5 hours expected value = 3
	1 x EdU + 1 x BrdU	2 x EdU + 1 x BrdU	2 x EdU + 1 x BrdU
LSK	1.47 ± 0.85	4.47 ± 0.18	2.98 ± 0.19
LS⁻K	1.11 ± 0.15	4.64 ± 0.12	2.97 ± 0.04
CMP	1.64 ± 0.34	4.72 ± 0.11	3.00 ± 0.07
GMP	1.97 ± 0.39	4.63 ± 0.15	2.96 ± 0.15
MEP	0.97 ± 0.03	4.57 ± 0.10	2.97 ± 0.09

Figure 2. Optimization of EdU-BrdU dual labeling technique applied to HSPC in-vivo A, *Dual-deoxynucleoside labeling with single EdU (1.5 mg/mouse) and single BrdU dose (2 mg/mouse) separated by 2 hours (T_I). Bone marrow cell were harvested 0.5 hours after BrdU administration*. B, *Dual-deoxynucleoside labeling with two doses of EdU (2 x 1.5 mg/mouse) and single dose of BrdU (2 mg/mouse)*. C, *Representative dot-plots of Lin⁻cKit⁺ cells and EdU/BrdU fractions frequency in three experimental settings*. D, *Ratio of S-phase exiting cells (EdU⁺BrdU⁻) to S-phase entering cells (EdU⁻BrdU⁺) in three experimental settings determined in LSK cells, LS⁻K cells and their CMP, GMP and MEP subpopulations. Four to six mice were analyzed in each of the experimental settings. The experimentally obtained ratios were tested by Student's t-test (one sample, two-tailed) to the expected theoretical ratio of 4.0 or 3.0 (see text). The ratios were significantly different ($P < 0.05$) from 4.0 in the left two columns. Results in the table are mean ± SEM.*

shows representative EdU-BrdU plots for the three experimental settings.

The optimized DNA-labeling method, using two doses of EdU given 1 hour apart and T_I set at 1.5 hours, is graphically shown in Supplementary Figure 2. This experimental setting has been further used to determine the duration of the S-phase in various types of HSPCs, the cell flow rate into the G2-phase of the cell cycle, and for calculating the duration of their cell cycles.

S-phase duration in HSPCs

The labeling of cells with EdU and BrdU in the cell nucleus in parallel with the staining of cell membrane markers was verified by imaging flow cytometry (Figure 3(a)).

The S-phase cell duration was determined in all LSK cells and all LS^-K cells, in the LS^-K cells also in their three subtypes: CMPs, GMPs and MEPs. The S-phase duration ranged from 6.3 ± 0.5 hours in GMPs to 9.8 ± 0.7 hours in MEPs (Figure 3(b)).

Cell flow rate into G2-phase and duration of the cell cycle

The EdU^+BrdU^- cell fraction shows the rate at which cells leave the S-phase and enter the G2-phase, i.e. the cell flow rate in tetraploid (4n) cells. Assuming that all cells proliferate, we calculated the average cell cycle duration (T_C) in various types of HSPCs as $T_C = 100\% \times T_I/EdU^+BrdU^-$ % (Figure 4).

Cell numbers generated by mitotic division do not correspond to the number of cells entering G2-phase

Further, we estimated the number of cells generated by the mitotic division of cells previously labeled in the S-phase of the same cell cycle. We pulse-labeled DNA-synthesizing cells in mice with a single dose of BrdU injected 1.5–4.5 hours prior to bone marrow collection and examined $BrdU^+$ cells with the diploid (2n) DNA content (Supplementary Figure 3). $BrdU^+$ diploid cells (Figure 5(b)) appeared 1.5 hours after BrdU administration (Figure 5(a)) and their number increased linearly until 4.5 hours (Figure 5(c)).

Our expectation that the increment in 2n $BrdU^+$ cells per hour, i.e. the cell flow rate into the (G0)G1-phase, should be twice as high as the cell flow rate into the G2-phase in particular cell types, due to the doubling effect of mitosis was not confirmed. Our experimental data differed from this theoretical value of 2.0 both in LSK cells, where it was only 1.1, and also in LS^-K cells, where it was 2.4–2.9 (Figure 5(d)).

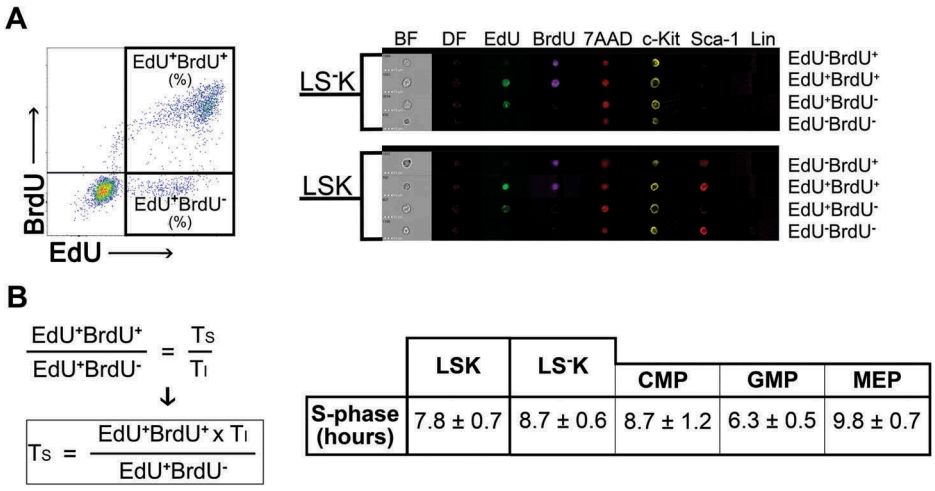

	LSK	LS⁻K	CMP	GMP	MEP
S-phase (hours)	7.8 ± 0.7	8.7 ± 0.6	8.7 ± 1.2	6.3 ± 0.5	9.8 ± 0.7

Figure 3. EdU-BrdU dual labeling of LSK and LS-K cells and its use to estimate duration of the S-phase A, *Representative example of $Lin^-c\text{-}Kit^+$ cells plotted on EdU vs. BrdU diagram and examples of surface antigen staining combined with DNA-labeling with EdU and BrdU as shown by imaging flow cytometry. 7AAD was used as a nuclear marker.* B, *Duration of S-phase (T_S) was determined in six mice (female) given two doses of EdU and a single dose of BrdU with a T_I = 1.5 hours (see Figure 2B). The calculation of T_S is based on the fact that the EdU^+BrdU^- cells indicate the fraction of S-phase cells exiting the S-phase within 1.5 hours (T_I). The total number of S-phase cells is then indicated by EdU^+BrdU^+ cells (see part 2 of Results). The results in the table are mean ± SEM from the six mice analyzed also in Figure 2.*

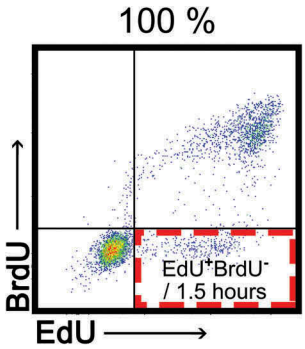

$$Tc = \frac{100\ \%}{EdU^{+}BrdU^{-}\ /\ hour}$$

	$EdU^{+}BrdU^{-}$ per hour (%) (cell flow rate per hour)	Average Tc (hours)
LSK	2.2 ± 0.2	47.0 ± 4.9
$LS^{-}K$	4.3 ± 0.5	23.4 ± 2.3
CMP	2.4 ± 0.4	42.5 ± 7.3
GMP	4.0 ± 0.4	24.9 ± 2.2
MEP	6.0 ± 0.5	16.7 ± 1.3

Figure 4. Cell flow rate into G2-phase and average cell cycle time in LSK and LS-K cells *The percentage of $EdU^{+}BrdU^{-}$ cells appearing per hour indicates the cell flow rate in the cell cycle. The cell cycle time, T_C, is then calculated as 100%/cell flow rate per hour (%). The T_C values thus represent an average values of cell cycle duration under the simplification assuming that all cells continuously cycle. Duration of cell cycle (T_C) was determined in six mice (female) given two doses of EdU and a single dose of BrdU with T_I = 1.5 hours (see Figure 2B). Results are mean ± SEM from six mice analysed also in Figures 2 and 3.*

Estimation of cell production in HSPCs

Previous results showed that almost half of LSK cells lost the Sca-1 antigen after mitotic division because the cell flow rate into G2-phase was only 1.1 times that in the preceding G2-phase, instead of the expected value of 2.0. This corresponds to asymmetric cell division where one cell replaces the cell that had divided and the other cell differentiates into another ($LS^{-}K$) cell type. In contrast, in $LS^{-}K$ cells and in their CMPs, GMPs and MEPs

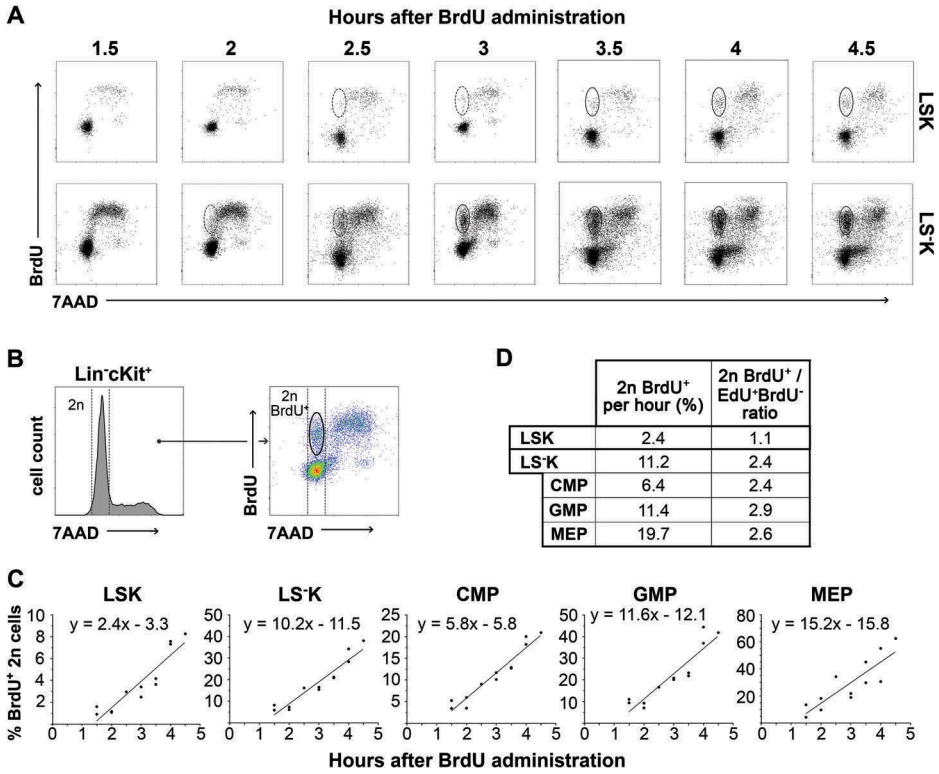

Figure 5. BrdU labeled diploid (2n) HSPCs in bone marrow collected between 1.5–4.5 hours after a single dose of BrdU A, *Representative examples of diploid (2n) daughter cell appearance in LSK and $LS^{-}K$ cells in increasing time intervals after in-vivo BrdU administration (i.v., 1.5 mg/mouse). Presented dotplots are from two independent experiments.* B, *Representative 7AAD histogram and BrdU/7AAD dotplot of $Lin^{-}cKit^{+}$ cells depicting gating strategy for 2n daughter cells.* C, *Changes in 2n $BrdU^{+}$ cells frequency depending on time elapsed since BrdU administration. Results from three independent experiments were pooled. The points were fitted to a line by linear regression, and the equations of increasing line are listed in graphs (n = 12).* D, *2n $BrdU^{+}$ increment per hour, i.e. G1 flow rate, determined according to curve slopes and ratio of G1 flow rate vs G2 flow rate for each HSPC type.*

subtypes, the cell flow rate into the G1-phase was more than 2.0 times that in the preceding G2-phase, which indicated that a majority of the LS$^-$K cells arising from mitotic division entered a new round of the cell cycle while both preserving their phenotype, i.e. the mitosis was symmetric and self-renewing. Furthermore, there is indication for an additional external influx of LS$^-$K cells, presumably from a part of LSK cells that lost Sca-1 marker after/during mitosis. This interpretation of our experimental data analyzing the flow rate of LSK and LS$^-$K cells into the G2- and G0/G1-phases, essential for estimation of the cell production rates in LSK and subtypes of LS$^-$K cells, is shown diagrammatically in Figure 6(a).

The calculation of cell production rates used the total number of a particular cell type in bone marrow (N) determined from the number of the cells in the femoral bone marrow multiplied by 15 (bone marrow in 1 femur represents ≈ 6.7% of the total bone marrow [13]). Other experimentally determined values used for estimation of the cell production rate in subtypes of Lin$^-$c-Kit$^+$ immature hematopoietic cells were their cell flow rates into the G2- (G2) and G1-phases (G1) of the cell cycle and the G1/G2 ratio (R). The cells produced per hour in the entire bone marrow are then calculated as N x G2 x R/100. The estimates of the cells produced in LSK cells and three types of LS$^-$K cells are presented in Figure 6(b). For comparison, the estimate of the total production of the mature myeloid cells derived from their numbers in blood and their replacement rates [13,14] is presented as well.

Discussion

The hematopoietic tissue is characterized by intensive cell proliferation resulting in the lifelong production of mature blood cells. The longevity of blood cell production is due to the presence of HSCs possessing both self-renewal and multilineage differentiation potential. However, HSCs in the bone marrow of adult mice divide very rarely [23–25]. Therefore, HSCs are linked to blood cell production through actively proliferating progenitor cells. We attempted to estimate the quantitative contribution of various types of these immature hematopoietic cells to steady-state murine hematopoiesis. Although the proliferation rate of these cells has been characterized previously [24,26], the available data were insufficient for estimating the number of cells produced. We decided to fill this gap in knowledge by determining the cell flow rates at

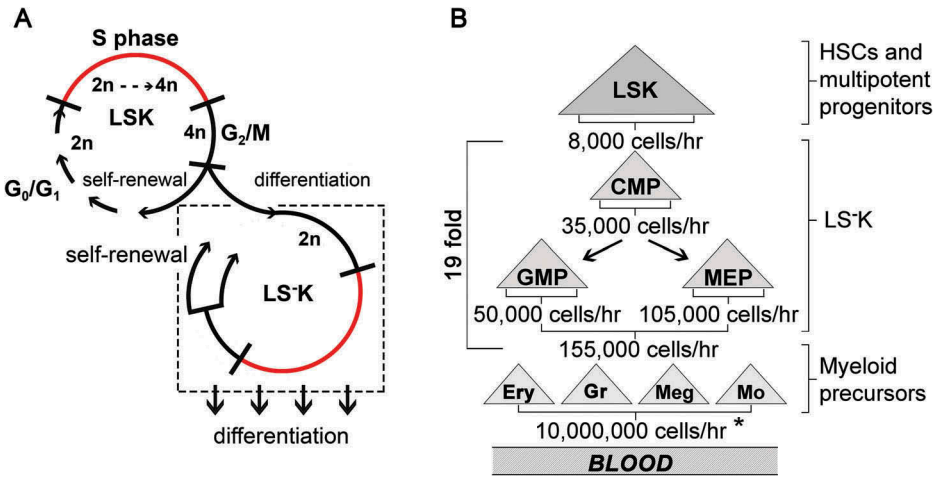

Figure 6. A model of self-renewal and differentiation in LSK and LS-K cells and estimation of cell production in hierarchy of HSPCs and myeloid precursors of blood cells A, *Cell division in LSK cells is primarily asymmetric when one cell becomes an LS$^-$K cell, while the other enters a new self-renewing cell cycle. LS$^-$K cells undergo self-renewal leading to their amplification and receive an influx of cells from the asymmetrically dividing LSK cells. The differentiation of LS$^-$K cells is not linked to cell division.* B, *Developmental hierarchy within HSPCs with established cell production rates and the average multiplication factor in the compartment of LS$^-$K cells and in the maturing precursors of red blood cells, granulocyte/monocytes and megakaryocytes. The cells produced per hour are calculated as described in Results. Briefly, the absolute number of various types of HSPCs determined in the femoral bone marrow was multiplied by 15 to estimate their absolute numbers in whole bone marrow (N). This was multiplied by the cell flow rate into G2-phase (G2) (see Figure 4) and further by the ratio of the cell flows in G1- and G2-phases of the cell cycle (see Figure 5) reflecting their mitotic multiplication efficiency. * estimated in Novak & Necas 1994 and Necas et al., 1995.*

which various types of immature hematopoietic cells progress through the cell cycle. These enabled us to determine the duration of the S-phase and to calculate the average cell cycle time in LSK cells and in three subtypes of LS$^-$K cells: CMPs, GMPs and MEPs.

To achieve this goal, we first had to optimize the method of sequential dual labeling of DNA-synthesizing cells. We noticed that when bone marrow cells were labeled with single doses of EdU and BrdU with a 2 hours interval between them and collected 0.5 hours after BrdU administration (Figure 2(a)), the fraction of the cells labeled only by BrdU almost equaled that of cells labeled only by EdU. This strongly suggested that the period when cells incorporated EdU was shorter than the two-hour period preceding BrdU administration. We concluded that the short EdU labeling period led to the underestimation of the fraction of EdU$^+$BrdU$^+$ cells because some cells had started DNA synthesis when EdU was no longer available. We have resolved this issue by adding a second EdU injection 0.5 hours before BrdU injection. BrdU is preferentially incorporated into the DNA in presence of EdU [27], and therefore only a negligible amount of EdU could have been incorporated after BrdU administration in our experiments. However, even if EdU had continued to be incorporated into DNA-synthesizing cells in parallel with BrdU, this would have overestimated the double-labeled fraction of EdU$^+$BrdU$^+$ cells very little as the 0.5h interval is much shorter than the total duration of S-phase, which is several hours.

Further, we were concerned with the possibility that some EdU$^+$BrdU$^-$ cells which exited from S-phase after the first dose of EdU could have divided within two and half hours, thereby artificially increasing number of EdU$^+$BrdU$^-$ cells. Therefore, we determined the ratio of EdU$^+$BrdU$^-$ to EdU$^-$BrdU$^+$ cells and compared it with a theoretical ratio corresponding to equal labeling periods for EdU and BrdU. Results of this comparison suggested that a part of EdU$^+$BrdU$^-$ cells indeed could have divided. Therefore, we shortened the interval between the first EdU injection and the BrdU injection to 1.5 hours, which suppressed this distortion.

The recently published study by Akinduro et al. [20] used the dual sequential EdU-BrdU labeling to determine the flow rate of cells entering S-phase, i.e. the EdU$^-$BrdU$^+$ fraction. This study assumed that EdU was available for DNA synthesis for only ≈ 0.5 hours after its administration, which is consistent with our findings. Importantly, the proportion of LSK cells entering S-phase determined in the Akinduro study (1–3.5% per hour), was similar to the flow rate of cells exiting S-phase measured by us (2.2% per hour), further confirming our results.

After establishing the number of HSPCs leaving the S-phase and entering the G2-phase of the cell cycle, we decided to check the obtained values by independently determining the number of daughter cells arising from their mitotic division. Previous results indicated that 4n cells entering the G2-phase started to divide approximately 1.5 hours later, which resulted in reduction of their DNA content to 2n values. Their number should have doubled if both daughter cells had maintained the phenotype of the mother cell. The DNA content reduced from 4n to 2n values allowed their clear distinction by flow cytometry. Therefore, we measured the increment of cells with 2n DNA content labeled with BrdU during the preceding S-phase.

The obtained experimental results significantly differed from the expectation that both daughter cells arising from mitosis would maintain the phenotype of the mother cell. Furthermore, they differed in the opposite ways in LSK and LS$^-$K cells. While newly-produced 2n LSK cells were only 1.1 times of their cell flow into the G2-phase, there were seemingly more than 2.0 times in newly-produced LS$^-$K cells. Neither of the values fitted the model of one cell giving rise to two identical daughter cells during its division. Almost one half of the total progeny of LSK cells lost the LSK phenotype, which strongly suggested they differentiated in mitosis. Moreover, there must have been an external external source of influx of 2n LS$^-$K cells in addition to their generation by their own cell division. This led us to formulate a model in which LSK cells self-renew and differentiate into LS$^-$K cells by predominantly asymmetric cell divisions (Figure 6(a)).

The resulting ratio of the 2n BrdU$^+$ cell flow rate into the G1-phase and the EdU$^+$BrdU$^-$ cell flow rate into the G2-phase exceeding in LS$^-$K cells the theoretical value 2.0, corresponding to the mitotic doubling

effect, was the major challenge in interpretation and understanding our experimental data. This comprise CMPs, GMPs and MEPs. We tentatively attributed this phenomenon to the influx of cells from the LSK cell compartment into LS-K cells. However, in hierarchical model of hematopoiesis, this influx should affect only CMPs but not GMPs and MEPs. The influx of cells from LSK population, arising from asymmetric mitosis (Figure 6(a)), into the G1-phase of CMPs could explain the exceedance of the theoretical value 2.0 for CMPs. Therefore, it remained to explain the exceeded theoretical value 2.0 for GMPs and MEPs. These cells could obtain a cell influx from amplified CMPs similarly as the influx into CMPs from differentiated LSK. Another or additional explanation could be the differentiation of GMPs and MEPs occurring during S-phase. This differentiation would diminish the cell flow rate into the G2-phase. The distorted ratio of G1/G2 flow rates can also lead to the values > 2.0. In this regard, it is important that Pop et al. [28] and Hwang et al. [29] demonstrated that in the fetal liver, immature hematopoietic cells achieve the erythroid phenotype during the S-phase of the cell cycle.

Our research designed primarily to establish the quantitative cell production in various types of hematopoietic progenitor cells has achieved this goal, as summarized in Figure 6(b). It confirmed the role of $LS^{-}K$ cells in the main amplification stage in the production of blood cells. It also resulted in the refinement of the labeling methods, enabling analysis of the cell cycle characteristics of hematopoietic cells *in vivo*. Unexpectedly, it revealed the significant difference in how the Sca-1^{+} and Sca-1^{-} subsets of immature hematopoietic cells self-renew and differentiate. This novel discovery points to the specific roles of these two hierarchically linked cell types in hematopoiesis. While the LSK cells maintain their population size and differentiate to $LS^{-}K$ cells by asymmetric cell divisions, the $LS^{-}K$ cells primarily amplify their numbers by symmetric self-renewing cell divisions to provide cells that are capable of further differentiation under local and external cues reflecting the immediate needs for specific blood cell types.

Summary

Paral et al. optimize the double-pulse DNA-labeling technique for *in-vivo* study of hematopoiesis and determine the cell cycle parameters and cell production rates in stem and progenitor cells, further reveal the different way in which Sca-1^{+} and Sca-1^{-} progenitors self-renew and differentiate.

Highlights

The fraction of DNA-synthesizing cells is a characteristic feature of various HSPCs.

The double-pulse DNA-labeling requires optimization for *in-vivo* use.

A half of Sca-1^{+} progenitors lose Sca-1 during mitosis.

The Sca-1^{-} progenitors amplify their numbers by symmetric self-renewing mitoses.

Author contributions

PP designed and performed experiments, analyzed data and prepared manuscript

KF analyzed data and prepared manuscript

MM collected and analyzed flow cytometry data

NR analyzed data and prepared manuscript

LS analyzed data and prepared manuscript

EN designed experiments, interpreted data and prepared manuscript

Disclosure statement

No potential conflict of interest was reported by the authors.

Funding

The work was supported by the Grant Agency of the Czech Republic (GACR 17-01897S). It received also support from the Charles University (PROGRES Q26, SVV 260371/2017) and the National Program of Sustainability II (LQ1604) from the Ministry of Education and Sport of the Czech Republic.

ORCID

Petr Páral http://orcid.org/0000-0003-2308-9688
Kateřina Faltusová http://orcid.org/0000-0003-4260-8797
Martin Molík http://orcid.org/0000-0002-3028-8055
Nicol Renešová http://orcid.org/0000-0003-4397-9469
Luděk Šefc http://orcid.org/0000-0003-2846-220X
Emanuel Nečas http://orcid.org/0000-0002-6101-4639

References

[1] Spangrude GJ, Heimfeld S, Weissman IL. Purification and characterization of mouse hematopoietic stem cells. Science [Internet]. 1988 Jul 1;241(4861):58–62. [cited 2016 Sep 16]. Available from: http://www.ncbi.nlm.nih.gov/pubmed/2898810

[2] Ogawa M, Matsuzaki Y, Nishikawa S, et al. Expression and function of c-kit in hemopoietic progenitor cells. J Exp Med [Internet]. 1991 Jul 1;174(1):63–71. [cited 2016 Sep 19]. Available from: http://www.ncbi.nlm.nih.gov/pubmed/1711568

[3] Okada S, Nakauchi H, Nagayoshi K, et al. In vivo and in vitro stem cell function of c-kit- and Sca-1-positive murine hematopoietic cells. Blood [Internet]. 1992 Dec 15;80(12):3044–3050. [cited 2016 Sep 19]. Available from: http://www.ncbi.nlm.nih.gov/pubmed/1281687

[4] Osawa M, Hanada K, Hamada H, et al. Long-term lymphohematopoietic reconstitution by a single CD34-low/negative hematopoietic stem cell. Science [Internet]. 1996 Jul 12;273(5272):242–245. [cited 2016 Aug 18]. Available from: http://www.ncbi.nlm.nih.gov/pubmed/8662508

[5] Akashi K, Traver D, Miyamoto T, et al. A clonogenic common myeloid progenitor that gives rise to all myeloid lineages. Nature [Internet]. 2000 Mar 9;404 (6774):193–197. [cited 2016 Sep 19]. Available from: http://www.ncbi.nlm.nih.gov/pubmed/10724173

[6] Adolfsson J, Borge OJ, Bryder D, et al. Upregulation of Flt3 expression within the bone marrow Lin(-)Sca1(+) c-kit(+) stem cell compartment is accompanied by loss of self-renewal capacity. Immun [Internet]. 2001 Oct;15(4):659–669. [cited 2016 Sep 19]. Available from: http://www.ncbi.nlm.nih.gov/pubmed/11672547

[7] Na Nakorn T, Traver D, Weissman IL, et al. Myeloerythroid-restricted progenitors are sufficient to confer radioprotection and provide the majority of day 8 CFU-S. J Clin Invest [Internet]. 2002 Jun;109 (12):1579–1585. [cited 2016 Sep 16].Available from: http://www.ncbi.nlm.nih.gov/pubmed/12070305

[8] Mj K, Yilmaz OH, Iwashita T, et al. SLAM family receptors distinguish hematopoietic stem and progenitor cells and reveal endothelial niches for stem cells. Cell [Internet]. 2005;121(7):1109–1121.[cited 2016 Sep 16]. Available from: http://www.ncbi.nlm.nih.gov/pubmed/15989959

[9] Adolfsson J, Månsson R, Buza-Vidas N, et al. Identification of Flt3+ lympho-myeloid stem cells lacking erythro-megakaryocytic potential a revised road map for adult blood lineage commitment. Cell [Internet]. 2005 Apr 22;121(2):295–306. [cited 2016 Sep 19]. Available from: http://www.ncbi.nlm.nih.gov/pubmed/15851035

[10] Oguro H, Ding L, Morrison SJ. SLAM family markers resolve functionally distinct subpopulations of hematopoietic stem cells and multipotent progenitors. Cell Stem Cell [Internet]. 2013 Jul 3;13(1):102–116. [cited 2016 Sep 16]. Available from: http://www.ncbi.nlm.nih.gov/pubmed/23827712

[11] Goodell MA. Isolation and functional properties of murine hematopoietic stem cells that are replicating in vivo. J Exp Med [Internet]. 1996 Apr 1;183 (4):1797–1806. [cited 2017 Dec 18]. Available from: http://www.ncbi.nlm.nih.gov/pubmed/8666936

[12] Weksberg DC, Chambers SM, Boles NC, et al. CD150-side population cells represent a functionally distinct population of long-term hematopoietic stem cells. Blood [Internet]. 2008 Feb 15;111(4):2444–2451. [cited 2017 Dec 20]. Available from: http://www.ncbi.nlm.nih.gov/pubmed/18055867

[13] Novak JP, Necas E. Proliferation-differentiation pathways of murine haemopoiesis: correlation of lineage fluxes. Cell Prolif [Internet]. 1994 Oct;27(10):597–633. [cited 2016 Sep 16].

[14] Necas E, Sefc L, Brecher G, et al. Hematopoietic reserve provided by spleen colony-forming units (CFU-S). Exp Hematol [Internet]. 1995 Nov;23(12):1242–1246. [cited 2016 Aug 18]. Available from: http://www.ncbi.nlm.nih.gov/pubmed/7589277

[15] Sun D, Luo M, Jeong M, et al. Epigenomic profiling of young and aged HSCs reveals concerted changes during aging that reinforce self-renewal. Cell Stem Cell [Internet]. 2014 May 1;14(5):673–688. [cited 2016 Sep 16]. Available from: http://www.ncbi.nlm.nih.gov/pubmed/24792119

[16] Qiu J, Papatsenko D, Niu X, et al. Divisional history and hematopoietic stem cell function during homeostasis. Stem Cell Reports [Internet]. 2014 Apr 8;2 (4):473–490. [cited 2016 Sep 16]. Available from: http://www.ncbi.nlm.nih.gov/pubmed/24749072

[17] Busch K, Klapproth K, Barile M, et al. Fundamental properties of unperturbed haematopoiesis from stem cells in vivo. Nature [Internet]. 2015 Feb 11;518 (7540):542–546. [cited 2017 Jun 26]. Available from: http://www.nature.com/doifinder/10.1038/nature14242

[18] Schoedel KB, Morcos MNF, Zerjatke T, et al. The bulk of the hematopoietic stem cell population is dispensable for murine steady-state and stress hematopoiesis. Blood [Internet]. 2016 Nov 10;128(19):2285–2296. [cited 2018 Jan 11]. Available from: http://www.ncbi.nlm.nih.gov/pubmed/27357698

[19] Sawai CM, Babovic S, Upadhaya S, et al. Hematopoietic stem cells are the major source of multilineage hematopoiesis in adult animals. Immunity [Internet]. 2016 Sep 20;45(3):597–609. [cited 2017 Dec 12]. Available from: http://www.ncbi.nlm.nih.gov/pubmed/27590115

[20] Akinduro O, Weber TS, Ang H, et al. Proliferation dynamics of acute myeloid leukaemia and haematopoietic progenitors competing for bone marrow space. Nat Commun [Internet]. 2018 Dec 6;9(1):519. [cited 2018 Apr 15]. Available from: http://www.ncbi.nlm.nih.gov/pubmed/29410432

[21] Martynoga B, Morrison H, Price DJ, et al. Foxg1 is required for specification of ventral telencephalon and region-specific regulation of dorsal telencephalic precursor proliferation and apoptosis. Dev Biol [Internet]. 2005;283(1):113–127.[cited 2017 May 2]. Available from: http://www.ncbi.nlm.nih.gov/pubmed/15893304

[22] Massey AJ, Keijzer R, Velde CVD, et al. Multiparametric cell cycle analysis using the operetta high-content imager and harmony software with PhenoLOGIC. Cotterill S, editor. PLoS One [Internet]. 2015 Jul 28;10(7):e0134306. [cited 2017

Mar 10]. Available from: http://dx.plos.org/10.1371/journal.pone.0134306

[23] Wilson A, Oser GM, Jaworski M, et al. Dormant and self-renewing hematopoietic stem cells and their niches. Ann N Y Acad Sci [Internet]. 2007 Jun;1106:64–75. [cited 2016 Sep 16]. Available from: http://www.ncbi.nlm.nih.gov/pubmed/17442778

[24] Foudi A, Hochedlinger K, Van Buren D, et al. Analysis of histone 2B-GFP retention reveals slowly cycling hematopoietic stem cells. Nat Biotechnol [Internet]. 2009 Jan;27(1):84–90. [cited 2016 Sep 16]. Available from: http://www.ncbi.nlm.nih.gov/pubmed/19060879

[25] van der Wath RC, Wilson A, Laurenti E, et al. Estimating dormant and active hematopoietic stem cell kinetics through extensive modeling of bromodeoxyuridine label-retaining cell dynamics. PLoS One [Internet]. 2009;4(9): e6972.[cited 2016 Sep 16]. Available from: http://www.ncbi.nlm.nih.gov/pubmed/19771180

[26] Passegué E, Wagers AJ, Giuriato S, et al. Global analysis of proliferation and cell cycle gene expression in the regulation of hematopoietic stem and progenitor cell fates. J Exp Med [Internet]. 2005 Dec 5;202(11):1599–1611. [cited 2017 Oct 31]. Available from: http://www.ncbi.nlm.nih.gov/pubmed/16330818

[27] Bradford JA, Clarke ST. Dual-pulse labeling using 5-ethynyl-2′-deoxyuridine (EdU) and 5-bromo-2′-deoxyuridine (BrdU) in Flow Cytometry. In: Current Protocols in Cytometry [Internet]. Hoboken, NJ, USA: John Wiley & Sons, Inc; 2011. p. Unit 7.38. [cited 2018 Apr 15] . Available from: http://www.ncbi.nlm.nih.gov/pubmed/21207361

[28] Pop R, Shearstone JR, Shen Q, et al. A key commitment step in erythropoiesis is synchronized with the cell cycle clock through mutual inhibition between PU.1 and S-phase progression. PLoS Biol [Internet]. 2010;8(9). [cited 2018 Jan 11]. Available from: http://journals.plos.org/plosbiology/article/file?id=10.1371/journal.pbio.1000484&type=printable

[29] Hwang Y, Futran M, Hidalgo D, et al. Global increase in replication fork speed during a p57KIP2-regulated erythroid cell fate switch. Sci Adv [Internet]. 2017 May;3(5):e1700298. [cited 2018 Jan 11]. Available from: http://www.ncbi.nlm.nih.gov/pubmed/28560351

Supplementary material

Supplementary Figure 1

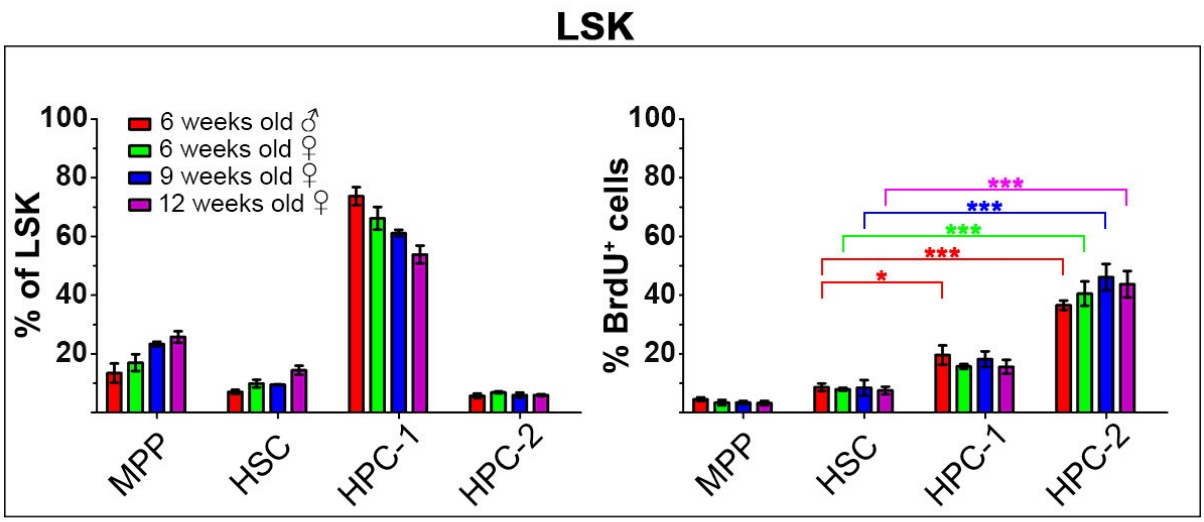

Frequency of four CD150/CD48 subpopulations of LSK cells and their proliferation rate assessed according to percentage of BrdU-positive cells.

Difference in % of BrdU-labeled cells was evaluated in all subpopulations compared to HSCs.

*Significant differences from HSCs are marked *p<0.001,***p<0.001.*

Supplementary Figure 2

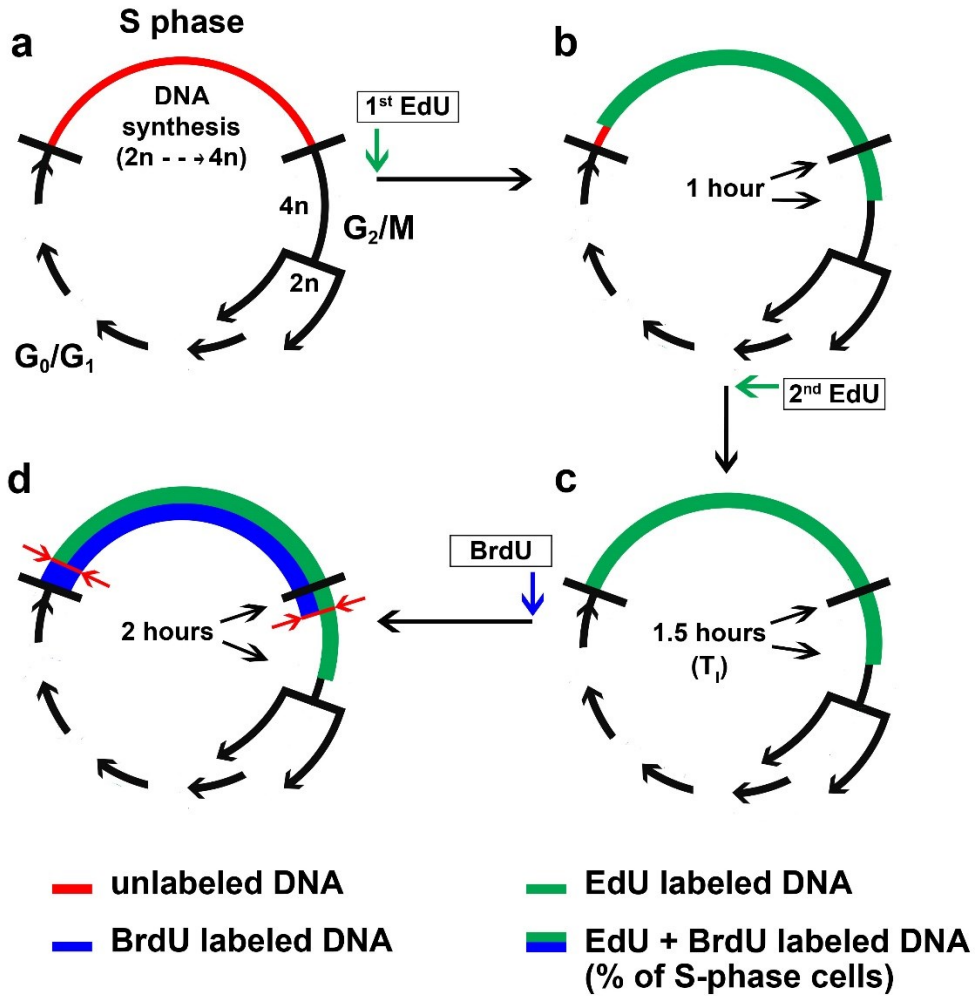

EdU – BrdU dual labeling of DNA optimized for *in-vivo* cell cycle analysis of HSPCs (2 x EdU, T_I = 1.5 hours).

a) *Cell cycle with highlighted S-phase (red)*

b) *EdU labels DNA (green) 0.5 hours after its administration and there are EdU unlabeled cells at the beginning of S-phase one hour after EdU (red)*

c) *2nd EdU dose, given 0.5 hour before BrdU, ensures that all DNA-synthesizing cells are labeled with EdU (green) during T_I*

d) *Half an hour after BrdU, all S-phase cells are double labeled by both EdU (green) and BrdU (blue). EdU-only labeled cells indicate the cells that exited from the S-phase during T_I. BrdU-only labeled cells (blue) represent cells entering the S-phase in the first half hour after BrdU administration.*

Supplementary Figure 3

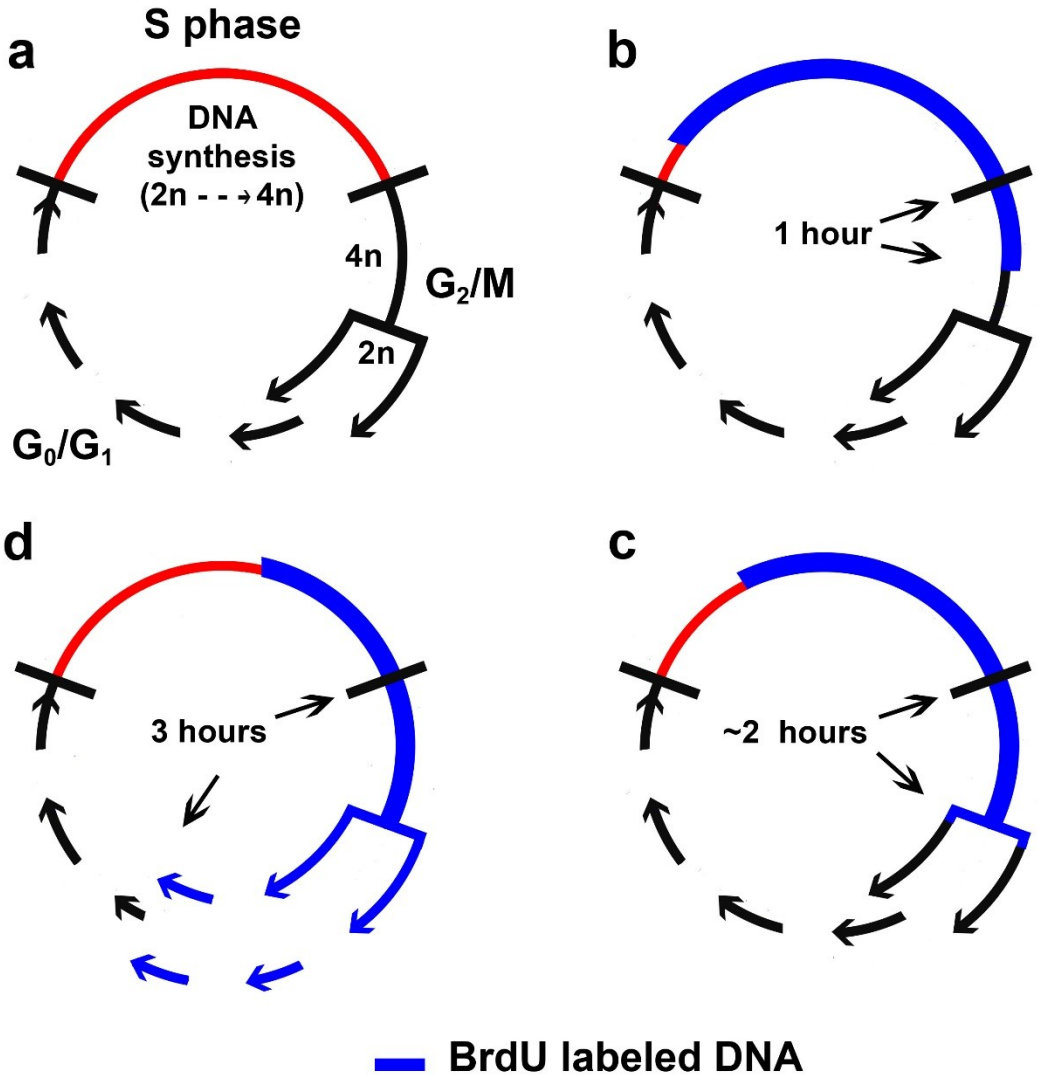

Time course of single (pulse) BrdU labeling.

a) *cells with unlabeled DNA*

b) *4n (G2/M) cell fraction increased in 1 hour after single BrdU dose*

c) *first 2n $BrdU^+$ cells appeared*

d) *2n $BrdU^+$ cell fraction increased in first 3 hours after single BrdU dose*

Supplementary Table 1

Antibodies	Source	Identifier
Alexa Fluor® 700 anti-mouse Lineage Cocktail	BioLegend	Cat#133313; components include anti-mouse CD3, clone 17A2; anti-mouse Ly-6G/Ly-6C, clone RB6-8C5; anti-mouse CD11b, clone M1/70; anti-mouse CD45R/B220, clone RA3-6B2; anti-mouse TER-119/Erythroid cells, clone Ter-119; N/A
FITC anti-mouse Lineage Cocktail	BioLegend	Cat#133302; components include anti-mouse CD3e, clone 145-2C11; anti-mouse Ly-6G/Ly-6C, clone RB6-8C5; anti-mouse CD11b, clone M1/70; anti-mouse CD45R/B220, clone RA3-6B2; anti-mouse TER-119/Erythroid cells, clone Ter-119; N/A
Biotin anti-mouse Lineage Panel	BioLegend	Cat#133307; components include anti-mouse CD3, clone 145-2C11; anti-mouse Ly-6G/Ly-6C, clone RB6-8C5; anti-mouse CD11b, clone M1/70; anti-mouse CD45R/B220, clone RA3-6B2; anti-mouse TER-119/Erythroid cells, clone Ter-119; N/A
Rat Brilliant Violet 421(TM) anti-mouse CD117 (c-Kit) Antibody, monoclonal	BioLegend	Cat#105827; clone 2B8; RRID: AB_10898120
Rat PE anti-mouse CD117 (c-Kit) Antibody, monoclonal	BioLegend	Cat#105808; clone 2B8; RRID: AB_313217
Rat APC/Cy7 anti-mouse Ly-6A/E (Sca-1) Antibody, monoclonal	BioLegend	Cat#108126; clone D7; RRID: AB_10645327
Rat PE anti-mouse Ly-6A/E (Sca-1) Antibody, monoclonal	BioLegend	Cat#122508; clone E13-161.7; RRID: AB_756193
Rat PE/Cy7 anti-mouse Ly-6A/E (Sca-1) Antibody, monoclonal	BioLegend	Cat# 122513; clone E13-161.7; RRID: AB_756198
Hamster PE/Cy7 anti-mouse CD48 Antibody, monoclonal	BioLegend	Cat#103424; clone HM48-1; RRID: AB_2075049
Rat PE anti-mouse CD150 (SLAM) Antibody, monoclonal	BioLegend	Cat#115904; clone TC15-12F12.2; RRID: AB_313683
Rat Brilliant Violet 785(TM) anti-mouse CD127 (IL-7Rα) Antibody, monoclonal	BioLegend	Cat#135037; clone A7R34; RRID: AB_2565269
Rat Brilliant Violet 510(TM) anti-mouse CD16/32 Antibody, monoclonal	BioLegend	Cat#101333; clone 93; RRID: AB_2563692
Rat APC anti-mouse CD16/32 Antibody, monoclonal	BioLegend	Cat#101336; clone 93; RRID: AB_1953273
Rat Biotin anti-mouse CD34 Antibody, monoclonal	Thermo Fisher Scientific	Cat#13-0341-82; clone RAM34; RRID: AB_466425
PE/Cy7 Streptavidin	BioLegend	Cat#405206; N/A

APC/Cy7 Streptavidin	BioLegend	Cat#405208; N/A
Brilliant Violet 605(TM) Streptavidin	BioLegend	Cat#405229; N/A
Mouse Pacific Blue BrdU Antibody, monoclonal	Thermo Fisher Scientific	Cat#B35129; clone MoBU-1; RRID: AB_2536433

Cell Cycle Analysis Using In Vivo Staining of DNA-Synthesizing Cells.

Páral P, Báječný M, Savvulidi F, Nečas E.

Methods Mol Biol. 2019. doi: 10.1007/7651_2019_228.

Link: https://www.ncbi.nlm.nih.gov/pubmed/31079341